Kinematic Analysis and Optimal Design of 3-PPR Planar Parallel Manipulator

Kee-Bong Choi*

Robot & Control Group, Intelligence & Precision Machine Dept., Korea Institute of Machinery and Materials 171, Jang-Dong, Yuseong-Gu, Daejeon, 305-343, Korea

This paper proposes a 3-PPR planar parallel manipulator, which consists of three active prismatic joints, three passive prismatic joints, and three passive rotational joints. The analysis of the kinematics and the optimal design of the manipulator are also discussed. The proposed manipulator has the advantages of the closed type of direct kinematics and a void-free workspace with a convex type of borderline. For the kinematic analysis of the proposed manipulator, the direct kinematics, the inverse kinematics, and the inverse Jacobian of the manipulator are derived. After the rotational limits and the workspaces of the manipulator are investigated, the workspace of the manipulator is simulated. In addition, for the optimal design of the manipulator, the performance indices of the manipulator are investigated, and then an optimal design procedure is carried out using Min-Max theory. Finally, one example using the optimal design is presented.

Key Words : Planar Parallel Manipulator, Kinematics, Jacobian, Workspace, Optimal Design, Min-Max

1. Introduction

Parallel manipulators consisting of closed-loop mechanisms have many advantages compared to serial manipulators in terms of payload, accuracy, and stiffness. It is well known that parallel manipulators have a higher payload-to-weight ratio, higher accuracy, and higher structural rigidity than serial manipulators (Ben-Horin et al., 1998). Recently some machine-tools (Kim et al., 2001 ; Wang et al., 2001) have been developed utilizing these advantages. A manipulator for fine motion (Ryu et al., 1997) also adopted the parallel mechanism rather than the serial one, since the parallel mechanism can be manufactured monolithically.

* **E-mail** : kbchoi@kimm.re.kr
TEL : +82-42-868-7132; **FAX** : +82-42-868-7135
Robot & Control Group, Intelligence & Precision Machine Dept., Korea Institute of Machinery and Materials 171, Jang-Dong, Yuseong-Gu, Daejeon, 305-343, Korea. (Manuscript **Received** May 22, 2002; **Revised** December 13, 2002)

Among the parallel manipulators, the planar parallel manipulator is a manipulator for plane motion. Planar parallel manipulators have two degree-of-freedom (DOF) motion ; that is two translations, or 3-DOF motion, consisting of two translations and one rotation. It is well known that (2^3-1) variations of 3-DOF planar parallel manipulators exist, which are RRR, RRP, RPR, RPP, PRR, PRP, and PPR, depending on the combinations of prismatic joints and rotational joints, excluding a PPP combination, where the prismatic and rotational joints are represented by P and R (Merlet, 1996 and 2000). The solutions of the direct kinematics for possible architectures of the planar parallel manipulators were also already proposed (Merlet, 1996), but more concrete solutions and kinematic analyses of the architectures are still required.

Most 3-DOF planar parallel manipulators have disadvantages that the manipulators have polynomial types of complex direct kinematics and small workspaces with useless voids as well as concave types of borderlines. As the order of

the polynomials of the direct kinematics increase, solving equations as well as choosing a proper solution becomes a great burden. Moreover the concave types of borderlines induce non-straight motions from a neighbor of the borderline to the others. Therefore it is important that a parallel manipulator has a closed type direct kinematics and a void-free workspace with a convex type borderline.

In this paper, a 3-PPR planar parallel manipulator, in which P is an active prismatic joint, is proposed to overcome the aforementioned disadvantages, *i.e.*, the proposed manipulator has a closed type direct kinematics and a void-free workspace with a convex type of borderline. For the kinematic analysis of this manipulator, first the direct kinematics, inverse kinematics, and inverse Jacobian of the proposed manipulator are derived. Second, rotational limits and workspaces are investigated. Also, for the optimal design of this manipulator, performance indices of the manipulator are investigated and then an optimal design procedure is carried out using Min-Max theory. Finally, one example using the optimal design is presented.

2. Description of 3-PPR Planar Parallel Manipulator

Figure 1 shows the schematic configuration of a 3-PPR planar parallel manipulator that consists of three active prismatic joints, three passive prismatic joints, three passive rotational joints, a moving plate, and links. The active joints can be actuated by electric rotational motors and ball screws for motion transformation. The three links for motion of the active joints are fixed to a base frame with two ends of each link. The degree of freedom (DOF) of the planar manipulator, m, is represented by (Merlet, 2000)

$$m=3(l-n-1)+\sum_{i=1}^{n} d_i \qquad (1)$$

where l is the number of rigid bodies, n is the number of joints, and d_i is DOF of joint i. Since this manipulator has eight rigid bodies including the base, and nine joints with a total of nine DOF, its DOF is three ; *i.e.*, two translations and one rotation on the plane. In addition, when the active joints of the manipulator are locked, the DOF of the manipulator becomes zero because the nine joints have only six DOF. Therefore this manipulator has three DOF when the active joints are activated, whereas it becomes a static structure when the active joints are locked.

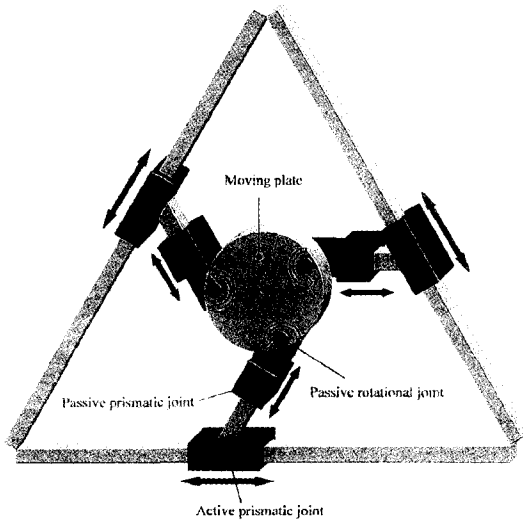

Fig. 1 Schematic configuration of 3 PPR planar manipulator

3. Direct Kinematics

The coordinates and the geometric parameters of this manipulator are shown in Fig. 2. The moving plate is a circle, which contains an equilateral triangle, with a radius r. The centers of the rotational joints are on the vertices of the triangle. The active prismatic joints can travel on the sides of the outer equilateral triangle which contains a circle with radius R. When the coordinate of each active joint A_i is (x_i, y_i), where $i=1$, 2, and 3, the moving plate has the pose of translation (x, y) and rotation ϕ from the reference point O. Then each length of the passive link becomes L_i. Because the inner and outer triangles are equilateral, the angle of the triangles, θ_0, is

$$\theta_0=\pi/3 \qquad (2)$$

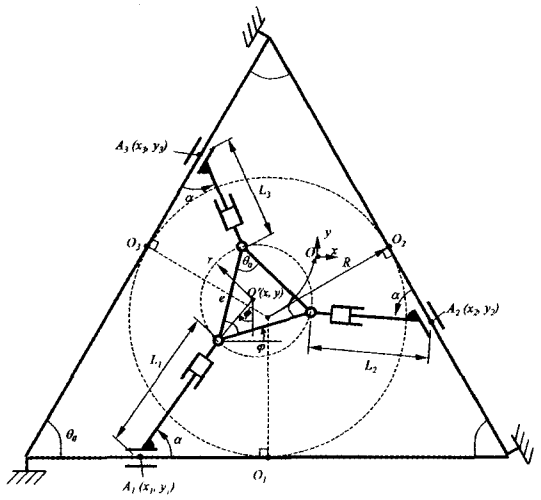

Fig. 2 Coordinate system for direct kinematics

The side length of the inner triangle, e, is

$$e=\sqrt{3}\,r \tag{3}$$

The incline of the inner triangle, φ, is expressed by the term of rotation of the moving plate, ϕ,

$$\varphi=\phi+\frac{\pi}{3} \tag{4}$$

The relative displacements of the active joints are

$$L_1\cos\alpha+e\cos\varphi+L_2\cos(\alpha-\theta_0)=x_2-x_1 \tag{5}$$

$$L_1\sin\alpha+e\sin\varphi+L_2\sin(\alpha-\theta_0)=y_2-y_1 \tag{6}$$

$$L_1\cos\alpha+e\cos(\theta_0+\varphi)+L_3\cos(\alpha+\theta_0)=x_3-x_1 \tag{7}$$

$$L_1\sin\alpha+e\sin(\theta_0+\varphi)+L_3\sin(\alpha+\theta_0)=y_3-y_1 \tag{8}$$

From Eqs. (5) and (6), the lengths L_1 and L_2 are

$$L_1=\frac{\cos(\alpha-\theta_0)}{\sin\theta_0}(y_2-y_1-e\sin\varphi)-\frac{\sin(\alpha-\theta_0)}{\sin\theta_0}(x_2-x_1-e\cos\varphi) \tag{9}$$

$$L_2=\frac{1}{\cos(\alpha-\theta_0)}(x_2-x_1-e\cos\varphi)-\frac{\cos\alpha}{\sin\theta_0}(y_2-y_1-e\sin\varphi)+\frac{\cos\alpha}{\sin\theta_0}\tan(\alpha-\theta_0)(x_2-x_1-e\cos\varphi) \tag{10}$$

Also, from Eqs. (7), (9), and (10), the length L_3 is

$$L_3=\frac{1}{\cos(\alpha+\theta_0)}\{x_3-x_1-e\cos(\theta_0+\varphi)\}-\frac{\cos(\alpha-\theta_0)\cos\alpha}{\cos(\alpha+\theta_0)\sin\theta_0}(y_2-y_1-e\sin\varphi)+\frac{\sin(\alpha-\theta_0)\cos\alpha}{\cos(\alpha+\theta_0)\sin\theta_0}(x_2-x_1-e\cos\varphi) \tag{11}$$

Substitution of Eqs. (9) ~ (11) into Eq. (8) derives the following equation:

$$C_1+C_2\cos\varphi+C_3\sin\varphi=0 \tag{12}$$

where

$$\begin{aligned}C_1&=\cos(\alpha+\theta_0)(y_3-y_1)-\sin(\alpha+\theta_0)(x_3-x_1)\\&\quad+\cos(\alpha-\theta_0)(y_2-y_1)-\sin(\alpha-\theta_0)(x_2-x_1)\\C_2&=e\{\sin\alpha+\sin(\alpha-\theta_0)\}\\C_3&=-e\{\cos\alpha+\cos(\alpha-\theta_0)\}\end{aligned} \tag{13}$$

Equation (12) can be solved introducing a parameter T as follows:

$$T=\tan\left(\frac{\varphi}{2}\right)$$
$$\cos\varphi=\frac{1-T^2}{1+T^2} \tag{14}$$
$$\sin\varphi=\frac{2T}{1+T^2}$$

Substituting Eq. (14) into Eq. (12), a second order polynomial in T is obtained as

$$(C_1-C_2)T^2+2C_3T+(C_1+C_2)=0 \tag{15}$$

Equation (15) offers the closed form solutions of T

$$T=\frac{-C_3\pm\sqrt{C_3^2+C_2^2-C_1^2}}{C_1-C_2} \tag{16}$$

From Eqs. (4) and (14), the rotation of the moving plate is

$$\phi=\tan^{-1}\left(\frac{2T}{1-T^2}\right)-\frac{\pi}{3} \tag{17}$$

Thus, the translation of the moving plate is

$$\begin{aligned}x&=x_1+L_1\cos\alpha-r\sin\phi\\y&=-R+L_1\sin\alpha+r\cos\phi\end{aligned} \tag{18}$$

It is remarkable that this manipulator has at most two solutions for direct kinematics according to Eq. (16), and moreover the closed-form solutions of Eqs. (17) and (18).

4. Inverse Kinematics and Inverse Jacobian

Figure 3 shows a coordinate system for describing the inverse kinematics of a 3-PPR planar parallel manipulator. When the center of the moving plate moves from origin O to O' with translation (x, y) and rotation ϕ, the vertex of the plate B_i is expressed as

$$\begin{aligned} x_{Bi} &= x + r\sin(\theta_i + \phi) \\ y_{Bi} &= y + r\cos(\theta_i + \phi) \end{aligned} \tag{19}$$

where

$$\theta_i = \frac{2(i-1)}{3}\pi \tag{20}$$

and $i=1, 2, 3$. The origin of the active prismatic joint O_i is departed by R from the origin O.

Provided that $\mathbf{u}_i$ and $\mathbf{v}_i$ are the unit vectors of the axes ξ_i and ζ_i, which are the axes of the active prismatic joint, the coordinate of the vertex B_i, expressed by the terms of ξ_i and ζ_i, is

$$\begin{aligned} \xi_{Bi} &= \overline{OB_i}\cdot\mathbf{u}_i \\ \zeta_{Bi} &= R + \overline{OB_i}\cdot\mathbf{v}_i \end{aligned} \tag{21}$$

Thus the position of the active prismatic joint, ξ_{Ai}, is

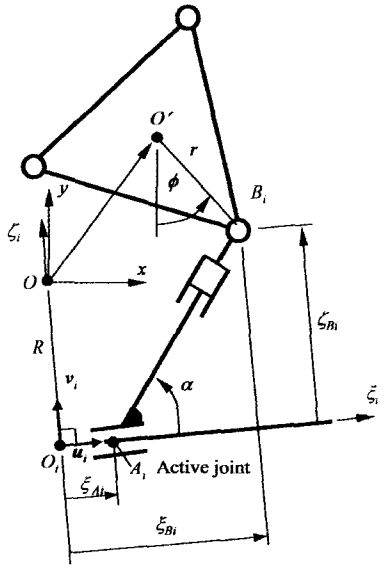

Fig. 3 Coordinate system for inverse kinematics

$$\xi_{Ai} = \xi_{Bi} - \zeta_{Bi}\cot\alpha \tag{22}$$

Direct differentiation of Eq. (22) with respect to the pose (x, y, ϕ) derives the inverse Jacobian $\mathbf{J}^{-1}$ as follows:

$$\mathbf{J}^{-1} = \begin{bmatrix} 1 & -\cot\alpha & r(\cos\phi - \cot\alpha\sin\phi) \\ \frac{1}{2}(-1+\sqrt{3}\cot\alpha) & \frac{1}{2}(\sqrt{3}+\cot\alpha) & r(\cos\phi - \cot\alpha\sin\phi) \\ -\frac{1}{2}(1+\sqrt{3}\cot\alpha) & \frac{1}{2}(-\sqrt{3}+\cot\alpha) & r(\cos\phi - \cot\alpha\sin\phi) \end{bmatrix} \tag{23}$$

The elements of the inverse Jacobian of Eq. (23) do not have the same dimension. First two columns corresponding to translation are dimensionless, whereas the last column corresponding to rotation has the dimension of length. By making the third column dimensionless, a homogeneous inverse Jacobian with non-dimensional elements is obtained by (Byun, 1997)

$$\mathbf{J}_h^{-1} = \mathbf{J}^{-1}\begin{bmatrix} 1 & 0 & 0 \\ 0 & 1 & 0 \\ 0 & 0 & 1/R \end{bmatrix} \tag{24}$$

5. Rotational Limit and Workspace

The rotation of the moving plate is restricted by the interference between the links and the rotational joints. Fig. 4 shows the configuration of this manipulator with rotational limits of the clockwise case (a) and counter clockwise case (b). Assuming the width of the links is negligible, the rotation ϕ is bounded by

$$-\frac{4}{3}\pi + \alpha \le \phi \le \frac{\pi}{3} + \alpha \tag{25}$$

Provided that ϕ_0 is the initial rotation defined by

$$\phi_0 = \alpha - \frac{\pi}{2} \tag{26}$$

The rotation range (25) is modified as

$$-\frac{5}{6}\pi \le \psi \le \frac{5}{6}\pi \tag{27}$$

where

$$\psi = \phi - \phi_0 \tag{28}$$

It is concluded that the moving plate of the 3-PPR planar parallel manipulator is bounded by $\pm 5\pi/6$ from the initial rotation.

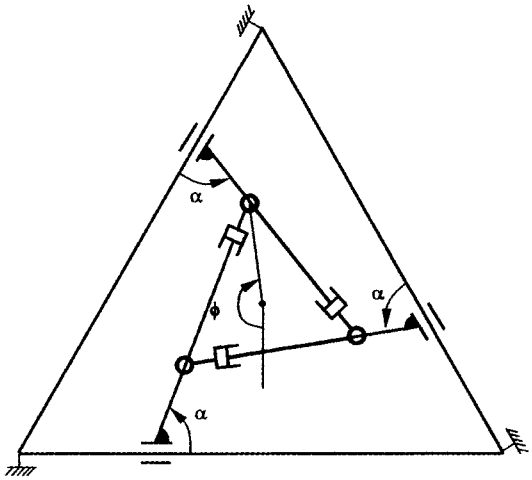

(a) Clockwise directional rotation limit

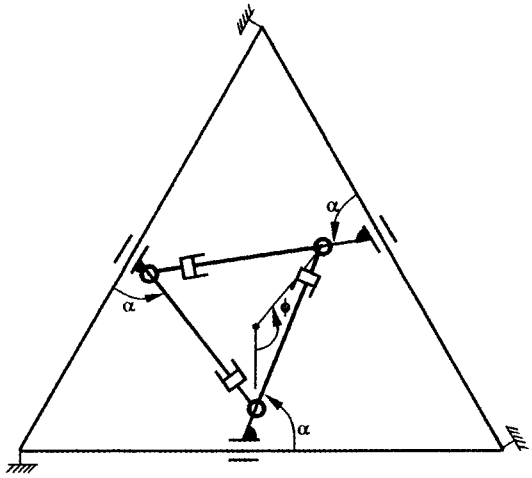

(b) Counter clockwise directional rotation limit

Fig. 4 Rotational limit

Provided that each active joint can move along the side of the equilateral triangle with a perpendicular distance R from the center of the triangle to the active joint, as shown in Fig. 2, and the moving range of the active joints is $2\sqrt{3}R$. Then, the center of the moving plate can reach a positional space within only some rotations in the rotational range (27), or can reach a fully rotatable positional space in the rotational range (27). The former is referred to as a reachable workspace and the latter is a dexterous workspace. Fig. 5 shows the reachable workspaces and the dexterous workspaces when r/R is 0.3, 0.5, 0.7, and α is $\pi/2$. The dexterous workspaces

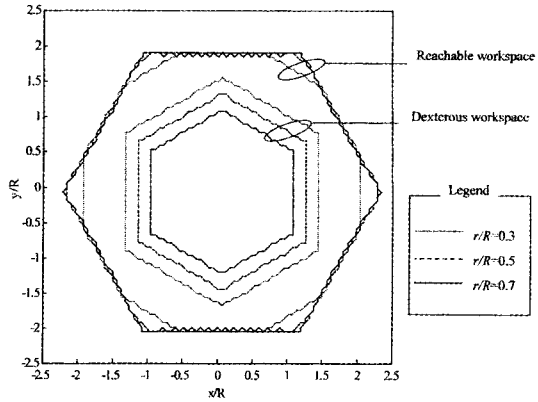

Fig. 5 Workspaces at $\alpha=\pi/2$

show a set of the reachable workspaces. As r/R increases, the reachable workspace increases slightly but the dexterous workspace decreases. Also, it is shown that the workspaces do not contain any voids, and moreover they have convex types of borderlines.

6. Local Performance Indices Using Inverse Jacobian

The inverse Jacobian provides information on the quality of the kinematical structure of a parallel manipulator. In this paper, manipulability, resistivity, and isotropy by using the inverse Jacobian are considered as performance indices of this parallel manipulator.

Manipulability, which is the distance from a singularity (Nakamura, 1991), evaluates the kinematic quality like the articular speed (Yoshikawa, 1990) of a manipulator. That is, the farther the configuration of the manipulator is from the singularity, the faster the manipulator moves. Smaller manipulability indicates that there is a singularity near the configuration of the manipulator. Thus, it is better to have maximal manipulability.

The manipulability of a parallel manipulator, w_m, is defined by

$$w_m=\sqrt{\det(\mathbf{J}_h^{-1}\mathbf{J}_h^{-T})} \tag{29}$$

In the non-redundant case, the manipulability w_m reduces to

$$w_m=|\det(\mathbf{J}_h^{-1})| \tag{30}$$

The determinant of the homogeneous inverse Jacobian is

$$\det(\mathbf{J}_h^{-1}) = \frac{3\sqrt{3}}{2}\frac{r}{R}(\cos\phi - \cot\alpha\sin\phi)(1+\cot^2\alpha) \quad (31)$$

From Eq. (31), the determinant of the homogeneous inverse Jacobian is shown to be independent of the position of the moving plate, but only dependant on ϕ and α. In addition, the determinant becomes zero at $\phi=\alpha$, that is $\psi=\pm\pi/2$. The 3-PPR planar parallel manipulator has a singular configuration at $\psi=\pm\pi/2$.

Resistivity w_r evaluates the articular force and is defined by the inverse of the manipulability as follows (Byun, 1997):

$$w_r = \frac{1}{|\det(\mathbf{J}_h^{-1})|} \quad (32)$$

The resistivity is correspondent to the force transmission ratio, which is the actuator capacity for a unit operational load (Lee at al., 2001). In the view of robustness of a mechanism, large resistivity is preferred. However, the resistivity increases abruptly at the neighborhood of a singular configuration, and the mechanism has a significant risk of breakdown at such a configuration. Therefore the design of the mechanism must be considered in terms of a compromise between manipulability and resistivity.

Isotropy corresponding to the inverse of the condition number is defined by the ratio of the minimum singular value to the maximum one of the inverse Jacobian (Nakamura, 1991), and is defined as follows (Liu at al., 2000):

$$w_i = \frac{1}{\|\mathbf{J}_h\|\,\|\mathbf{J}_h^{-1}\|} \quad (33)$$

where $\|\mathbf{J}_h\| = \sqrt{\mathrm{tr}(\mathbf{J}_h\mathbf{N}\mathbf{J}_h^T)}$ and $\mathbf{N} = \frac{1}{n}\mathbf{I}$ when n is the dimension of the inverse Jacobian. Manipulability is related to the magnitude of the manipulability ellipsoid, whereas the condition number concerns the shape of the ellipsoid (Nakamura, 1991). Isotropy evaluates workspace quality and prefers a sphere-like shape, *i.e.*, unity.

Fig. 6 shows the simulation results of local performance indices (manipulability, resistivity, and isotropy) with respect to α and ψ at $r/R=0.5$. In this study, ψ is bounded by Eq. (27) and α is restricted by

$$\frac{\pi}{6} \le \alpha \le \frac{5}{6}\pi \quad (34)$$

The local performance indices are symmetrical to $\psi=0$ and $\alpha=\pi/2$. Manipulability is zero at $\psi=\pm\pi/2$, increases as ψ is far from $\pm\pi/2$, and

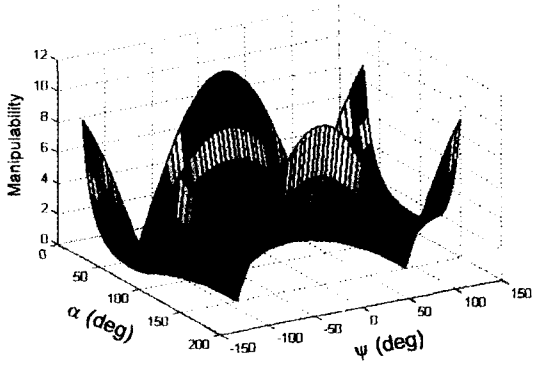

(a) Manipulability

Infinity

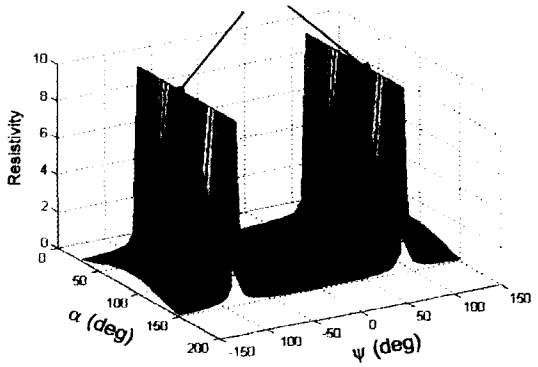

(b) Resistivity

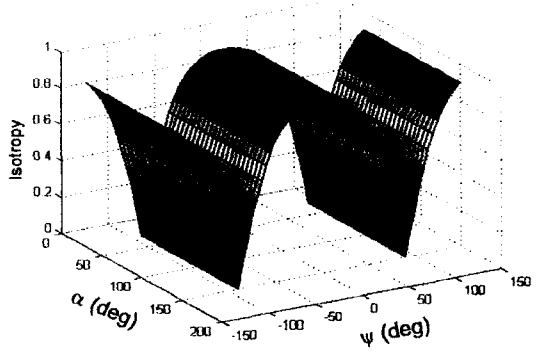

(c) Isotropy

Fig. 6 Local performance indices using inverse Jacobian at $r/R=0.5$

is maximal at $\psi=0$ in the range $-\pi/2<\psi<\pi/2$. This means that, in the view of manipulability, the manipulator prefers configurations far from $\psi=\pm\pi/2$. Conversely, resistivity is infinite at $\psi=\pm\pi/2$, and abruptly decreases as it is far from $\pm\pi/2$. Also, it has maximal values at $\alpha=\pi/2$ and decreases as α is far from $\pi/2$. Isotropy depending on only ψ rather than α is zero at $\psi=\pm\pi/2$, increases as ψ is far from $\pm\pi/2$, and is maximal at $\psi=0$ in the range $-\pi/2<\psi<\pi/2$.

7. Optimal Design

From the analyses of the above indices, the range of rotation ψ is agreeable to be $-\pi/2<\psi<\pi/2$, even though the rotational limit is expressed by the range of Eq. (27), because the singularity is at $\pm\pi/2$. In this study, the range of ψ is limited by

$$-\frac{17}{36}\pi\leq\psi\leq\frac{17}{36}\pi \tag{35}$$

for realistic implementation. Therefore the rotation range for the dexterous workspace is also modified by the range of Eq. (35). The performance indices on the workspace are chosen as the dexterous workspace within the rotation range of Eq. (35) and the difference in the size of the reachable workspace and the dexterous workspace along α and r/R.

Figure 7 shows the size of the reachable workspace, the size of the dexterous workspace and the difference in the size of the two workspaces with respect to α and r/R based on a constraint as follows:

$$0.1\leq\frac{r}{R}\leq1.0 \tag{36}$$

The size of the reachable workspace decreases as α keeps away from $\pi/2$ and increases slowly as r/R increases. The size of the dexterous workspace decreases, as α is far from $\pi/2$ and r/R increases. The difference in the size of the two workspaces decreases as α is far from $\pi/2$, and increases as r/R increases. In this study, a large size of the dexterous workspace and a small difference in the size of two workspaces are preferred.

A global performance index using an inverse Jacobian is expressed by an average local performance index on the total pose in the workspace. In this study, since the inverse Jacobian of this manipulator is not the function of translation but the function of rotation, the global performance index can be expressed by the average value on the range of Eq. (35). Fig. 8 shows the global

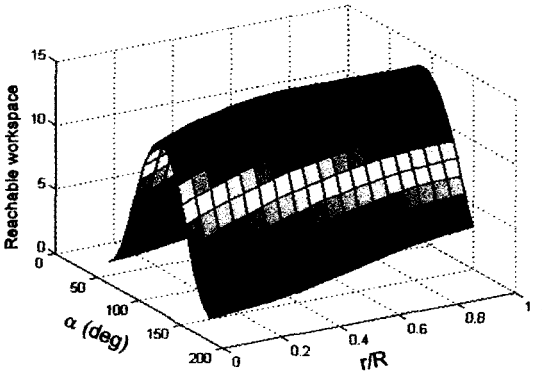

(a) Reachable workspace

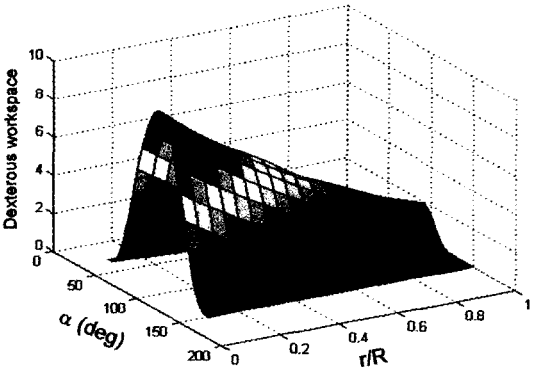

(b) Dexterous workspace

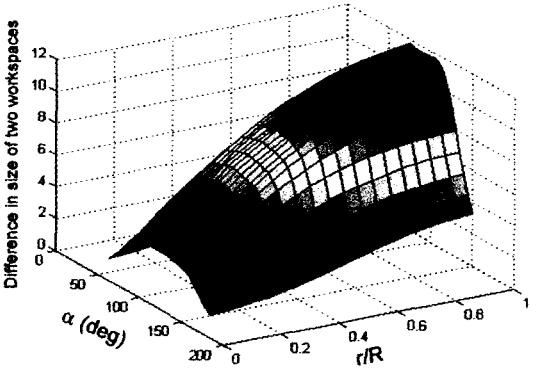

(c) Difference in the size of the reachable workspace and the dexterous workspace

Fig. 7 Workspaces

performance indices using the inverse Jacobian with respect to α and r/R. The global performance indices are symmetrical to $\alpha=\pi/2$. Manipulability increases as α is far from $\pi/2$ and r/R increases. The manipulability increases steeply as α is far from $\pi/2$ and r/R increases. In contrast to the manipulability, resistivity decreases as α is far from $\pi/2$ and r/R increases. Isotropy, depending on r/R rather than α, increases as r/R increases.

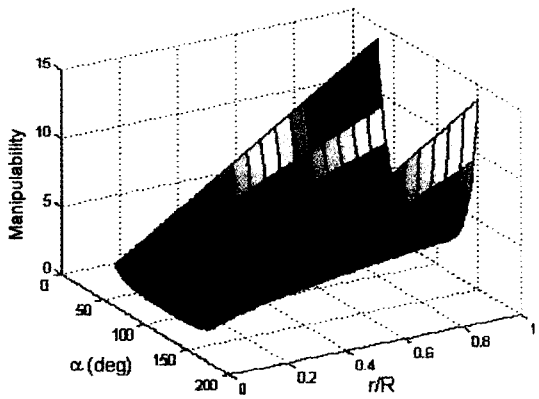

(a) Manipulability

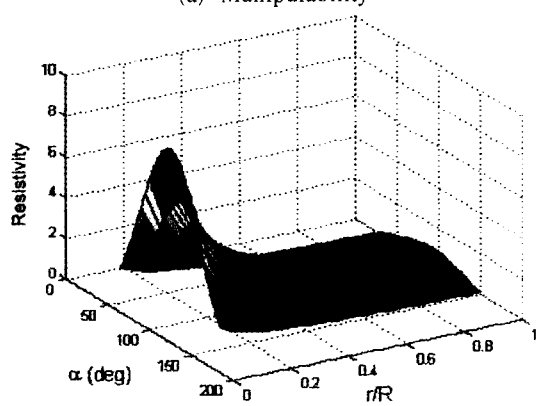

(b) Resistivity

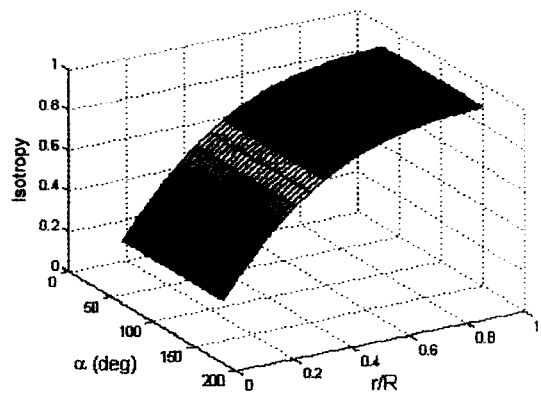

(c) Isotrophy

Fig. 8 Global performance indices using inverse Jacobian

A set of optimal design parameters is obtained using the Min-Max theory of fuzzy theory (Terano at al., 1992, Yi at al., 1994, and Lee at al., 1996) in a constraint space with respect to α and r/R. In addition, performance indices for the design parameters α and r/R are the dexterous workspace w_D, the difference in the size of the reachable workspace and dexterous workspace w_S, the global manipulability w_M, the global resistivity w_R, and the global isotropy w_I. Let $\bar{w}_j$, $\max(w_j)$, and $\min(w_j)$ be the normalized performance index, the maximum, and the minimum values of w_j in the given constraint space. Then the aforementioned performance indices are normalized by

$$\bar{w}_j=\frac{w_j-\min(w_j)}{\max(w_j)-\min(w_j)} \tag{37}$$

where the subscript j is D, M, R, and I, and

$$\bar{w}=\frac{\max(w_j)-w}{\max(w_j)-\min(w_j)} \tag{38}$$

where the subscript j is S. When the performance indices are weighted, the normalized performance indices are modified by

$$\tilde{w}_j=1+g_j(\bar{w}_j-1) \tag{39}$$

where $\tilde{w}_j$ is the weighted performance index and g_j is weight of the index with

$$0\le g_j\le 1 \tag{40}$$

In the given constraint space, a composite global performance index, W_c, can be found by the minimum set of the weighted performance indices as follows

$$W_c=\tilde{w}_D\wedge\tilde{w}_S\wedge\tilde{w}_M\wedge\tilde{w}_R\wedge\tilde{w}_I \tag{41}$$

where $\wedge$ means the fuzzy intersection. Then, the optimal design parameters are correspondent to the maximal position of the composite global performance index.

In summary, the described optimization problem can be written by

Find $(\alpha, r/R)$,

minimize $\dfrac{1}{(\tilde{w}_D \wedge \tilde{w}_S \wedge \tilde{w}_M \wedge \tilde{w}_R \wedge \tilde{w}_I)}$,

subject to $\dfrac{\pi}{6} \leq \alpha \leq \dfrac{5\pi}{6}$,

and $0.1 \leq \dfrac{r}{R} \leq 1.0$.

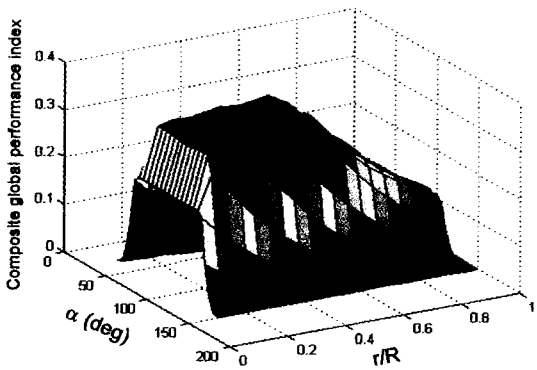

(a) Composite global performance index

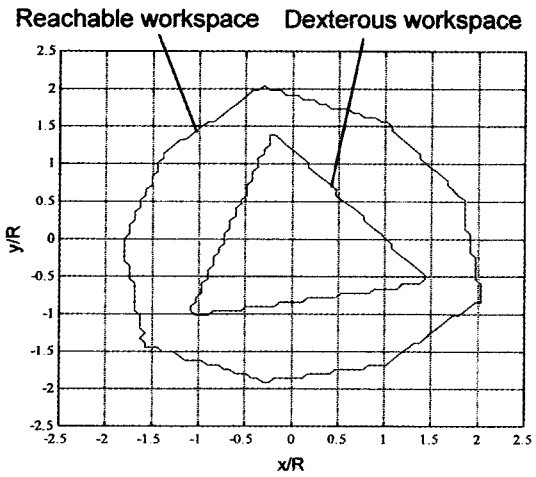

(b) Workspace

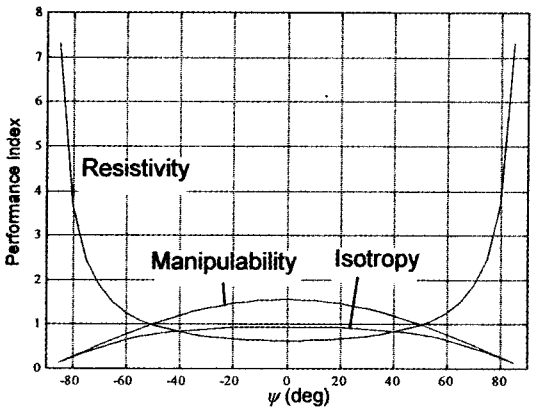

(c) Performance index

Fig. 9 Simulation results for optimal design

Figure 9 shows an optimal design example. Fig. 9(a) is the composite global performance index when the weights of the indices g_D, g_S, g_I, g_M, and g_R are 1.0, 0.9, 0.8, 0.7, and 0.6, respectively. Two sets of maximums in the map of the composite global performance index exist at $(\alpha, r/R) = (7\pi/18, 0.5)$ and $(11\pi/18, 0.5)$, because the map is symmetric to $\alpha = \pi/2$. The manipulator with these optimal design parameters α and r/R has the workspace shown in Fig. 9(b), and the performance index using the inverse Jacobian shown in Fig. 9(c).

8. Conclusions

A 3-PPR planar parallel manipulator has been proposed, and the analysis of the kinematics and the optimal design of the manipulator were discussed. The direct kinematics, the inverse kinematics, and the inverse Jacobian of the manipulator were derived. Also the workspace of the manipulator was simulated. For the optimal design of the manipulator, the performance indices were chosen as the size of the dexterous workspace, the difference in the sizes of the reachable workspace and the dexterous workspace, the manipulability, the resistivity, and the isotropy. The optimal design parameters were then obtained by the Min-Max theory, and one example was presented to show the validity of the optimal design.

From the kinematic analysis of the manipulator, we can draw the following conclusions:

(1) The DOF of this manipulator is three; *i.e.*, two translations and one rotation on a plane.

(2) This manipulator has a simple closed type of direct kinematics, inverse kinematics, and inverse Jacobian. In particular, the direct kinematics of this manipulator has at most two roots.

(3) Due to the interference between the links and the rotational joints, the moving plate of this manipulator is bounded by $\pm 5\pi/6$ from the initial rotation. Also it is shown that the workspaces of this manipulator do not contain any voids, and

moreover they have convex types of borderlines.

(4) This manipulator has a singular configuration at $\psi=\pm\pi/2$. The global performance indices are symmetrical to $\alpha=\pi/2$. Manipulability increases as α is far from $\pi/2$ and r/R increases. The manipulability increases steeply as α is far from $\pi/2$ and r/R increases. In contrast to the manipulability, resistivity decreases as α is far from $\pi/2$ and r/R increases. Isotropy, which depends on r/R rather than α, increases as r/R increases.

(5) This manipulator can be optimally designed by choosing proper weights for the performance indices by Min-Max theory.

References

Ben-Horin, R., Shoham, M. and Djerassi, S., 1998, "Kinematics, Dynamics and Construction of a Planarly Actuated Parallel Robot," *Robotics and Computer-Integrated Manufacturing*, Vol. 14, No. 2, pp. 163~172.

Byun, Y.-K., 1997, *Analysis and Design of a 6 Degree of Freedom 3-PPS(RRR)P Parallel Manipulator*, Ph. D. Dissertation in Korea Advanced Institute of Science and Technology.

Kim, J., Park, F. C., Ryu, S. J., Kim, J., Hwang, J. C., Park, C. and Iurascu, C. C., 2001, "Design and Analysis of a Redundantly Actuated Parallel Mechanism for Rapid Machining," *IEEE Transactions on Robotics and Automation*, Vol. 17, No. 4, pp. 423~434.

Lee, J. H., Yi, B.-J., Oh, S.-R. and Suh, I. H., 2001, "Optimal Design and Development of a Five-Bar Finger with Redundant Actuation," *Mechatronics*, Vol. 11, pp. 27~42.

Lee, S. H., Yi, B. J. and Kwak, Y. K., 1996, "Optimal Dynamic Design of Anthropomorphic Robot Module with Redundant Actuators," *KSME International Journal*, Vol. 10, No. 3, pp. 265~276.

Liu, X.-J., Jin, Z.-L. and Gao, F., 2000, "Optimal Design of a 3-DOF Spherical Parallel Manipulators with Respect to the Conditioning and Stiffness Indices," *Mechanism and Machine Theory*, Vol. 35, pp. 1257~12670.

Merlet, J.-P., 1996, "Direct Kinematics of Planar Parallel Manipulators," *Proceedings of the 1996 IEEE International Conference on Robotics and Automation*, Minneapolis, Minnesota, pp. 3744~3749.

Merlet, J.-P., 2000, *Parallel Robots*, Kluwer Academic Publishers.

Nakamura, Y., 1991, *Advanced Robotics Redundancy and Optimization*, Addison-Wesley Publishing Company.

Ryu, J. W., Gweon, D.-G. and Moon, K. S., 1997, "Optimal Design of a Flexure Hinge Based XYθ Wafer Stage," *Precision Engineering*, Vol. 21, pp. 18~28.

Terano, T., Asai, K. and Sugeno, M., 1992, *Fuzzy systems theory and its applications*, 1st ed. San Diego, Harcourt Brace Jovanovitch.

Wang, Z., Wang, Z., Liu, W. and Lei, Y., 2001, "A Study on Workspace, Boundary Workspace Analysis and Workpiece Positioning for Parallel Machine Tools," *Mechanism and Machine Theory*, Vol. 36, pp. 605~622.

Yi, B. J. and Kim, W. K., 1994, "Optimal Design of a Redundantly Actuated 4-Legged Six Degree of Freedom Parallel Manipulator Using Composite Design Index," *KSME International Journal*, Vol. 8, No. 4, pp. 385~403.

Yoshikawa, T., 1990, *Foundations of Robotics Analysis and Control*, The MIT Press Cambridge, Massachusetts London, England.